Instabilities in the flow of thin films on heterogeneous surfaces

Lou Kondic[a)]
Department of Mathematical Sciences & Center for Applied Mathematics & Statistics, New Jersey Institute of Technology, Newark, New Jersey 07102

Javier Diez[b)]
Instituto de Física Arroyo Seco, Universidad Nacional del Centro de la Provincia de Buenos Aires, Pinto 399, 7000, Tandil, Argentina

(Received 2 April 2004; accepted 21 May 2004; published online 28 July 2004)

We present computational and experimental results involving instability development in the gravity-driven flow of thin fluid films on heterogeneous surfaces, with particular emphasis on the dynamics of the fluid fronts. We show that heterogeneity of the solid surface can have a significant effect on the flow dynamics. Since the effect of heterogeneity often competes with the basic instability mechanism that would occur even on macroscopically homogeneous surfaces, the result is an elaborate interplay of various instability mechanisms. The computational results presented here outline both the flow on surfaces perturbed by regular patterns, and on surfaces perturbed by irregular, noiselike perturbations. We relate these computational results to the pattern formation process in our experiments of gravity-driven flow down an incline. Good qualitative agreement is found between the simulations and the experiments. © *2004 American Institute of Physics*. [DOI: 10.1063/1.1772732]

The flow of thin films is relevant in a number of different fields, such as engineering, biology, and chemistry. These flows can be driven by gravity, or various other forces of mechanical, thermal, or electromagnetic origins. In many situations, the fluid fronts become unstable, leading to the formation of fingerlike or triangular sawtooth patterns, and resulting in uneven or partial surface coverage. Very often, these instabilities are undesirable in technological applications since they may lead to the formation of dry regions or other defects. In other applications, however, partial wetting is actually preferred, since surfaces that are selectively wetted on microscale can be used as the base for various microelectromechanical system (MEMS) devices.

In this work, we concentrate on perhaps the simplest of thin-film flows, namely gravity-driven flow down an inclined plane. Experiments are usually performed by releasing fluid in some controllable fashion at the top of an incline. After some time, the initially straight contact line, where liquid, gas, and solid phases meet, becomes unstable with respect to transverse perturbations. It has been conjectured that this instability is related to the formation of a capillary ridge in the fluid profile, just behind the advancing contact line. Silvi and Dussan,[1] expanding on the pioneer work by Huppert,[2] show that the fluid wetting properties play an important role in the instability development and the degree of surface coverage. Recently, the experiments by Johnson and co-workers,[3,4] as well as computations by Diez and Kondic[5,6] show that another important parameter is the inclination angle. The decrease of the inclination angle not only reduces the patterns' growth rate, but it also modifies their shape: while larger angles lead to fingers characterized by almost straight sides, smaller angles lead to the formation of triangular sawtooth patterns.

Theoretically, the fluid film's dynamics are typically approached by using the lubrication approximation. Within this framework, an initial insight into the instability results from the linear stability analysis (LSA). Troian *et al.*[7] perform LSA for the flow down a vertical plane and show that there is a band of unstable modes, with short wavelengths being stabilized by surface tension. Spaid and Homsy[8] and Bertozzi and Brenner[9] extend this analysis to the general case of flow down an inclined plane, and show that the normal component of gravity (hydrostatic term) shifts the mode of maximum growth to longer wavelengths, and also tends to stabilize the flow by decreasing the instability's growth rate. This stabilizing effect appears to be so strong that it is predicted to completely remove the instability for very small inclination angles, in contradiction to experiments. In Ref. 9, a transient growth approach is used to explain this discrepancy, while Ye and Chang[10] use the spectral theory to reach the same goal. Both works analyze the propagation and amplification of noise from the substrate to the fluid front, although they employ different methods. Grigoriev[11] analyzes the transient growth and related effects in the flow of thermally driven films. A recent paper by Davis and Troian[12] claims that the influence of a transient growth mechanism is weaker than previously thought for gravity-driven thin films. Although our paper does not directly address the issue of transient growth, we expect that some results presented here will be of interest to that problem as well. We note that all computational works necessarily use one of two regularizing models to analyze the contact line dynamics: relaxing a no-slip boundary condition, and/or assuming a numerical precursor film.

The flow on heterogeneous surfaces has also been re-

a)Electronic mail: kondic@njit.edu
b)Electronic mail: jdiez@exa.unicen.edu.ar

cently considered by a number of authors. Kalliadasis *et al.*,[13] Bielarz and Kalliadasis,[14] and Decré and Baret[15] discuss two-dimensional (2D) and three-dimensional (3D) flow, respectively, over trenches that are of a comparable length scale to the film height, similarly to the earlier work by Stillwagon and Larson.[16] A concept of nonuniform slip coefficient has been applied to thin-film flows by Hoffman *et al.*[17] and Wang,[18] building upon previous works by Hocking[19] and Miksis and Davis.[20] Kondic and Diez[21] use a varied precursor film thickness to explore the instability development in the flow over controlled surface perturbations ("channels" of varying flow resistance). Modifications of the contact angle in the spreading of drops on chemically heterogeneous substrates are analyzed experimentally by Drelich *et al.*,[22] and computationally by Schwartz,[23] Schwartz and Elley,[24] and Brandon *et al.*[25] The effects of random distributions of perturbations at the substrate on the contact angle hysteresis has been discussed using the probability theory by Öpik.[26] A series of papers by Troian and co-workers[27–30] considers selective, controlled wetting of a chemically heterogeneous substrate. Garnier *et al.*[31] propose the use of thermal feedback control to suppress the contact line instability. Dewetting of heterogeneous substrates has been also analyzed recently, e.g., by Brusch *et al.*[32] and Kargupta and Sharma.[33] We will see later that some results presented in our work have common features to the results presented in Refs. 32 and 33, although the systems considered are rather different.

In this work, we concentrate on the influence of surface heterogeneity on the instability development. The heterogeneity, which in physical systems may be either due to noise, or due to imposed patterning, is modeled by perturbing the precursor film thickness. This simplified approach to the arguably quite complicated dynamics that occurs on a microscale is then used to discuss macroscale features of the instability development. This study is partially motivated by an earlier work by Kondic and Bertozzi[34] that has shown that substrate perturbations can play a role in the development of the instability. However, that work reached this conclusion indirectly, by recording the influence that a substrate perturbation has on the capillary ridge's height, which is itself related to the instability development. Here, we approach the instability directly, by performing fully nonlinear simulations in a 3D system under lubrication approximation. We note that in this work we assume complete wetting, and do not discuss in any detail issues related to nonzero contact angle. An interested reader can find significant material regarding partial wetting in recent works that discuss the disjoining-pressure model (e.g., Bertozzi *et al.*,[35] Glasner and Witelski[36]) or the related diffuse interface model (e.g., Pismen and Pomeau,[37] Thiele *et al.*[38]).

This paper is organized as follows. In Secs. I and II we formulate the problem and present computational and experimental results that outline the main features of the contact line instability in the flow on (macroscopically) homogeneous surfaces. In Sec. III we show in our simulations how a localized surface inhomogeneity, introduced by a perturbation of the precursor film thickness, leads to the formation of regular patterns. Section IV concentrates on the dynamics in systems with multiple perturbations, either discrete or continuous, including the modeling of random surface perturbations. The influence of boundary conditions, as well as parametric dependence, are discussed in Sec. V. In Sec. VI we use the understanding developed in the previous sections to approach a more involved problem of the interaction between multiple irregular ("noise") and regular (imposed patterns) surface perturbations both in simulations and in experiments. The experiments involve the flow of completely wetting viscous Newtonian fluid down a prewetted inclined plane in both (macroscopically) homogeneous and on patterned surfaces, prepared by introducing controlled, macroscopic regions of varied wetting properties. In both groups of experiments, the uncontrolled variations of the thickness of the prewetted film could be thought of as a source of the noise that we introduce in our numerical simulations. Although the physical mechanism by which the imposed perturbations modify the flow is different, we show that at least on a macroscopic level, these additional perturbations can also be successfully modeled by precursor film perturbations.

I. FORMULATION OF THE PROBLEM

The dynamics of thin liquid films is typically analyzed within the framework of the lubrication approximation. The assumptions of this approach, as well as the details of our computational methods are given elsewhere, see Diez and Kondic[39] and the references therein. For completeness, here we give a basic outline, concentrating mostly on the aspects relevant to the main subject of this work.

Within the lubrication approximation, one uses the fact that the film thickness is much smaller than any in-plane dimension. After depth averaging the fluid velocity over this short direction, and using a no-slip boundary condition at the solid–liquid interface, the continuity equation yields the following equation for the height h of the (incompressible) liquid film:

$$\frac{\partial h}{\partial t} = -\frac{1}{3\mu}\nabla\cdot[\gamma h^3\nabla\nabla^2 h - \rho g h^3\nabla h\cos\alpha + \rho g h^3\sin\alpha\mathbf{i}], \tag{1}$$

where $\nabla=(\partial_x,\partial_y)$, x points down the incline, and y points in the transverse direction. Here, μ, ρ, g, γ, and α are the viscosity, density, gravity, surface tension, and inclination angle, respectively. The fourth-order term results from surface tension, and the last two terms are due to gravity.

To balance viscous and capillary forces in Eq. (1), we scale h by the fluid thickness far behind the contact line, H, and define the scaled in-plane coordinates and time by $(\bar{x},\bar{y},\bar{t})=(x/X,y/X,t/T)$, where

$$X=\left(\frac{a^2H}{\sin\alpha}\right)^{1/3},\quad T=\frac{3\mu}{\gamma}\frac{a^2X}{H^2\sin\alpha}, \tag{2}$$

and $a=\sqrt{\gamma/\rho g}$ is the capillary length. The velocity scale is chosen naturally as $U=X/T$, and the capillary number is defined as $Ca=\mu U/\gamma$. Using this nondimensionalization, Eq. (1) for $\bar{h}=h/H$ is given by (dropping the bars)

$$\frac{\partial h}{\partial t} + \nabla \cdot [h^3 \nabla \nabla^2 h] - D(\alpha) \nabla \cdot [h^3 \nabla h] + \frac{\partial h^3}{\partial x} = 0, \quad (3)$$

where the single dimensionless parameter $D(\alpha) = (3Ca)^{1/3} \cot(\alpha)$ measures the size of the normal component of gravity.

All theoretical and computational methods require some regularizing mechanism. There are two commonly used approaches. The first one is to assume a small foot of fluid in front of the apparent contact line, the so-called precursor film, see Refs. 7–9. This model is also very well suited for the flows on prewetted surfaces (as considered in this work), where the numerical precursor film plays the role of the prewetting film in experiments. The second approach is to relax the no-slip boundary condition at the fluid–solid interface (see, e.g., Greenspan,[40] Dussan,[41] or Hocking and Rivers[42]). Diez *et al.*[43] have recently performed an extensive analysis of the computational performance of these regularizing mechanisms applied to the spreading drop problem. In that paper, it is shown that the results are rather insensitive to the choice of the model, consistent with, e.g., Ref. 8. However, the computational performance of the precursor film model is shown to be much better than that of various slip models.[43] This is an additional motivation for the use of a precursor film as a regularizing method. We note that the particular value of the precursor film thickness, b (scaled by H), influences the instability and the details of the evolving patterns. This point has recently been analyzed in some detail both experimentally[10] and computationally.[6] In Ref. 6 we show that the value $b=0.01$ is sufficiently small to correctly reproduce the main features of experimental results; therefore, this is the value that we use throughout this work.

The computational domain is chosen as a rectangle defined by $0 \leqslant x \leqslant L_x$ and $0 \leqslant y \leqslant L_y$, which is divided into $N_x \times N_y$ cells centered at node points (x_i, y_j) with $i=1,\ldots,N_x$ and $j=1,\ldots,N_y$. Equation (3) is then discretized in space by using a central finite difference scheme. The boundary conditions are chosen to model constant fluid flux far behind the fluid front. That is, we assume that there is an infinite stream of fluid far behind the front, that keeps the fluid height constant there. Within our nondimensionalization scheme, this leads to $h(0,y,t)=1$. We require that far ahead of the moving front, the fluid height is equal to the precursor thickness, $h(L_x,y,t)=b$, and also that the streamwise gradients of the fluid height vanish at the boundaries, i.e., $h_x(0,y,t) = h_x(L_x,y,t)=0$. At the boundaries $y=0$ and $y=L_y$, it is convenient to use $h_y(x,0,t)=h_y(x,L_y,t)=0$, $h_{yyy}(x,0,t) = h_{yyy}(x,L_y,t)=0$. This choice enforces that there is no flow across these boundaries. Since the tangential component of the fluid flux is let free (there is no adhesion of the fluid to the walls), these boundaries could be thought of as "slipping walls."

Time discretization is performed by using implicit Crank–Nicolson scheme. The advantages of an implicit scheme for this problem are obvious: the stability requirement for an explicit scheme is that $\Delta t < C \min[\Delta x, \Delta y]^4$, where Δt is a time step, and C is a positive constant. Thus, an explicit scheme requires very short time steps for a reasonable spatial accuracy. In our simulations, time steps are chosen dynamically, based on prescribed accuracy, and the obvious requirement that the computed solution is strictly positive.[39]

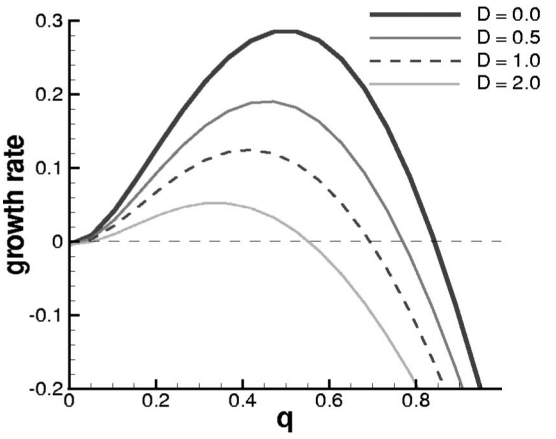

FIG. 1. Growth rate vs wave number for few different values of D.

The nonlinear system of algebraic equations that results after time discretization is linearized by using the Newton–Kantorovich method; the linearized problems are then solved by employing the iterative biconjugate gradient method. As a typical grid spacing, we use $\Delta x=0.2$, $\Delta y=0.25$, leading to about 200–400 grid points in each direction. More details regarding efficiency, computational cost, and other issues such as convergence and accuracy are given in Ref. 39.

II. MAIN FEATURES OF THE FLOW ON A HOMOGENEOUS SURFACE

Linear stability analysis[7–9] of the governing Eq. (3) has shown that the flow is unstable with respect to fluid front perturbations in the transverse direction. LSA is performed by expanding to the first order all nonlinear terms about the base state, obtained as the y-independent solution of Eq. (3) in a reference frame moving with velocity $u=1+b+b$.[27] It is characterized by the presence of a capillary ridge, which appears to be closely related to the onset of the instability.

Figure 1 illustrates the results of LSA, obtained by solving an eigenvalue problem of the form

$$Lg(\xi) = \sigma g(\xi),$$

where L is a linear operator whose coefficients depend on the base solution $h_0(\xi)$, and $\xi = x - c_0 t$. We solve this problem by following the method outlined in Ref. 10, and obtain the growth rate σ as the maximum value of the discretized spectrum. These calculations are performed with the routine RGG (EISPACK package) for q's in the range $0 \leqslant q \leqslant 1.2$.

Figure 1 shows that the long wavelengths are unstable, while the short ones are stabilized by surface tension, represented by the fourth-order term in Eq. (3). Consequently, there is a band of unstable modes bounded by the wave numbers $q=0$ and $q_c = 2\pi/\lambda_c$, where $\lambda_c \approx 8$ for $D=0$. The wavelength of maximum growth is approximately $\lambda_{\max} \approx 12-14$, and it grows as the inclination angle is decreased, or, equivalently, as the parameter D in Eq. (3) is increased. In the same time, the growth rate of the instability decreases as D is

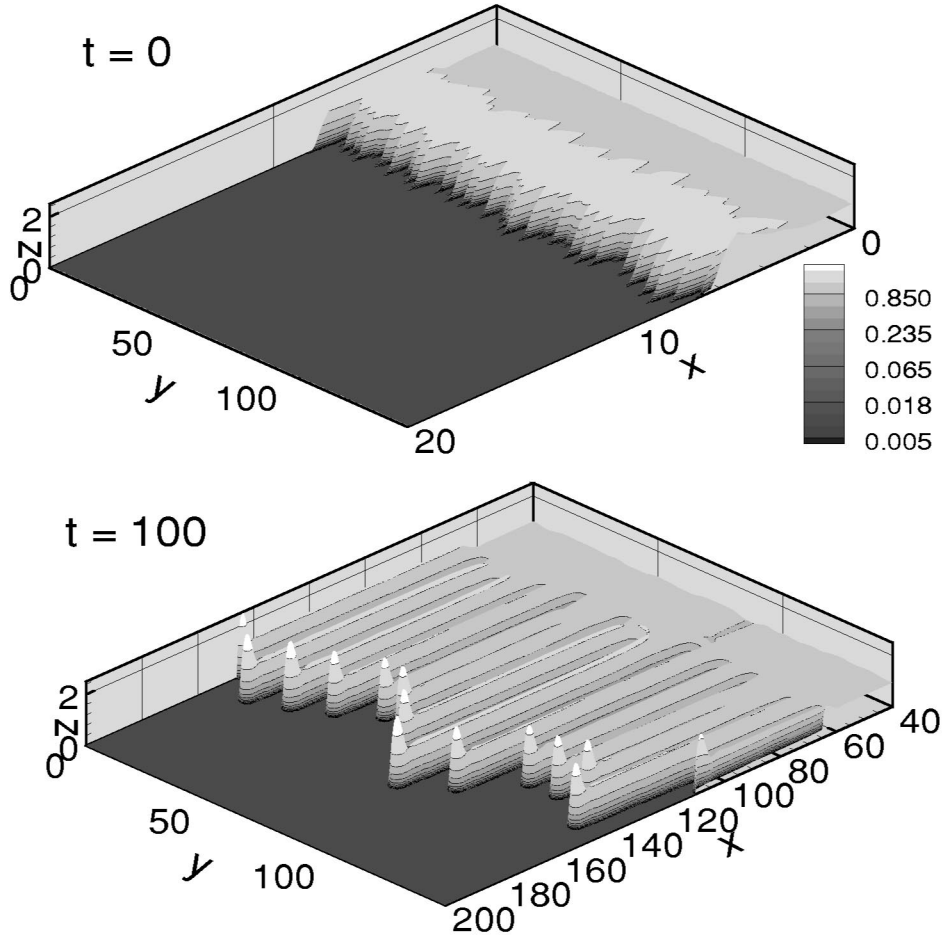

FIG. 2. Contour plot of the fluid thickness. The initial profile is perturbed by a superposition of 100 modes characterized by random amplitudes. Here $D=0$ and $b=0.01$. Note that the z scale is considerably stretched for presentation purposes ($L_y=144$).

increased. Although LSA is valid for short times only, one expects that the distance between the resulting patterns in actual experiments is close to $\lambda_{\max}$, and that the initial growth is approximately exponential with the growth rate close to $\sigma_{\max}$.

For future reference, we note here the influence of some of the parameters on the LSA results. An increase/decrease of the precursor film thickness leads to a decrease/increase of the growth rate of the emerging patterns. This observation was used in a recent work[21] which showed that perturbing precursor thickness in a controllable manner could induce instability and the occurrence of regular patterns. The influence of (noise-induced) precursor thickness perturbations on the flow stability for very small inclination angles was also analyzed in some detail in a number of recent works.[9,10,12,21]

Figure 2 shows an example of our recent computational results for the flow down a homogeneous vertical ($D=0$) substrate.[5,6] These results confirm the main predictions of LSA. Here, the initial condition is formulated by perturbing the base state [an example of a base state in 2D can be seen in Fig. 6(a)] by a superposition of $N=100$ modes characterized by wavelengths $\lambda_{0,i}=2L_y/i$, $i=1,\ldots,100$. Each mode is assigned a random amplitude in the range $[-0.1,0.1]$. This initial profile is shown in Fig. 2(a). In Fig. 2(b) we see the formation of long finger-like patterns that result for later times. These fingers are characterized by nonuniform lengths, resulting from the irregular initial conditions. This nonuniformity is also related to the fact that the distance between the fingers varies, although it is on average close to $\lambda_{\max}$ from LSA. Additional simulations that use different distributions of initial wavelengths and different domain size show that this average value is close to 12. More details regarding the influence of the inclination angle (controlled by the parameter D) on the pattern formation is available elsewhere.[5,6] Here, we provide a brief illustration by presenting the results of physical experiments.

The experiments are performed on a glass surface of dimensions of 100 by 50 cm, using fixed amount (typically, 25 g) of wetting fluid [polydimethylsiloxane (PDMS), AlfaAesar Ward Hill, MA], also known as silicon oil (viscosity: 50 cSt; surface tension: 21 dyn/cm, density 0.96 g/cm^3). The fluid is released close to the top of the plane by using a simple mechanical "dam" consisting of a piece of rubber fixed to a metal frame. The surface is prepared by cleaning it with soap and water. No efforts are made to remove PDMS from the previous runs from the glass surface, which can therefore be thought of as prewetted by the fluid. This applies to all of our experiments, including the ones performed on patterned surfaces shown later in Figs. 16–18. More details about experimental techniques, as well

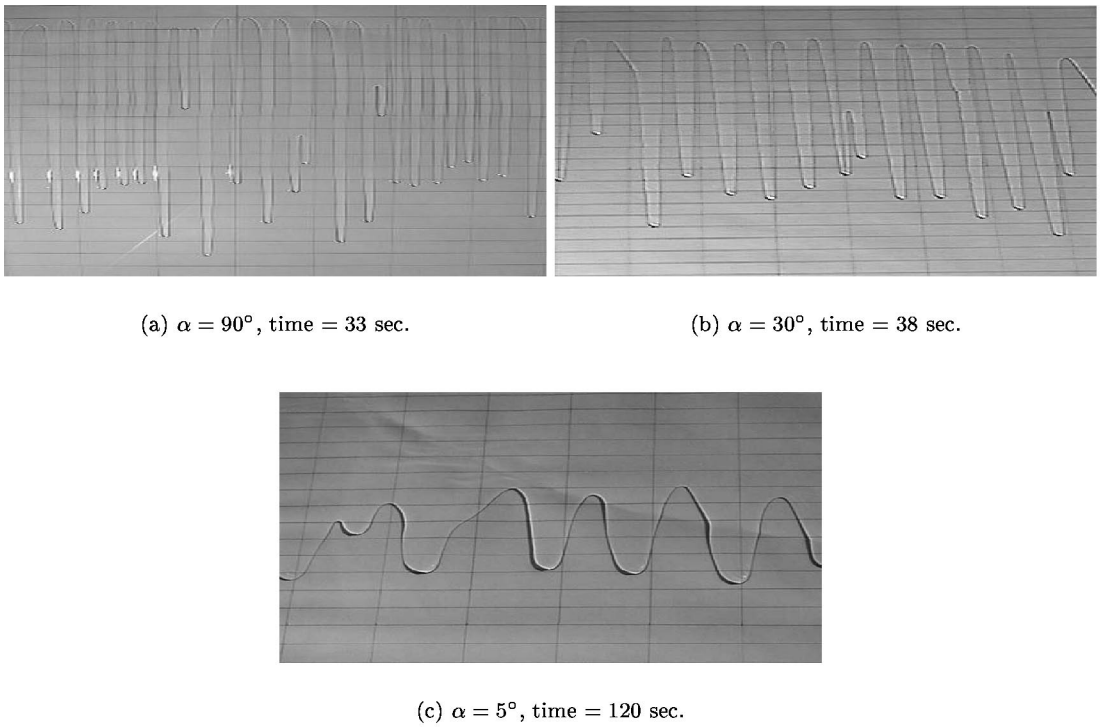

FIG. 3. Development of instability in physical experiments. Here, 25 g of PDMS is released at the top of a glass surface characterized by the inclination angle α. The rectangles' width (in the streamwise direction) is 2 cm, and their length is 5 cm.

as a pedagogical explanation of the details of the instability development, are available in the paper by Kondic.[44]

Figure 3 shows the developed patterns for three inclination angles: e.g., (a) $\alpha=90°$, (b) $\alpha=30°$, (c) and $\alpha=5°$. These results clearly show how the inclination angle influences the instability development: for smaller α (larger D), the instability develops slower, the wavelengths increase, and the evolving pattern shape changes smoothly from finger-like to triangular. These main features are in qualitative agreement with the computational results presented in Fig. 2 for $D=0$, and in Refs. 5 and 6 for $D>0$. For a more precise agreement, the simulations need to be adjusted for the fact that the experiments are performed using a finite amount of fluid. We analyze these issues elsewhere, and concentrate here on the constant flux flow on inhomogeneous surfaces.

Before proceeding, we note that LSA, as well as the computations such as those yielding the results presented in Fig. 2, assume the presence of small perturbations of the contact line in the transverse direction. These perturbations are necessarily present in any physical experiment. However, for simplicity of presentation, and since in this work we are predominantly interested in the inhomogeneities of surface itself, we mostly ignore these perturbations, and refer to them only briefly in connection to the experimental results presented in Sec. VI. Most of the computational results are obtained assuming $D=0$ (i.e., flow down a vertical plane), with the influence of nonzero D briefly outlined where appropriate so as to relate computations to experiments.

III. BASIC INSTABILITY MECHANISM OF THE FLOW ON INHOMOGENEOUS SURFACES

We model substrate inhomogeneity by perturbing the precursor film thickness. While it might appear that imposing perturbations of this kind is rather restrictive, since a precursor film is not always present in physical experiments or technological applications, this approach is actually quite general. Namely, a number of authors, including de Gennes,[45] have shown that the main flow features are not influenced significantly by the choice of the regularizing method at the contact line. One could allow for the presence of a precursor film, include the possibility of fluid slip, or assume that van der Waals forces at the liquid–solid interface are important; for the macroscopic flow properties (in particular, instability development), the main factor is the actual length scale that is introduced at the front. Since this length scale determines the degree of energy dissipation, one expects that its spatial variation can have a significant influence on the macroscopic flow properties, as shown in the case of the spatially dependent slip coefficient.[17,19]

A recent work[34] analyzed the influence that a localized perturbation of the precursor thickness had on the flow in 2D geometry (the y direction is ignored). Figure 4 shows an example of these results: as the fluid's main body flows over a perturbation (imposed at $x=20$ in Fig. 4), the capillary ridge's height is increased, implying, as pointed out above, that the flow stability properties may be modified. Correspondingly, it is reasonable to assume that surface inhomogeneities might lead to flow instabilities. Figure 4(a) shows

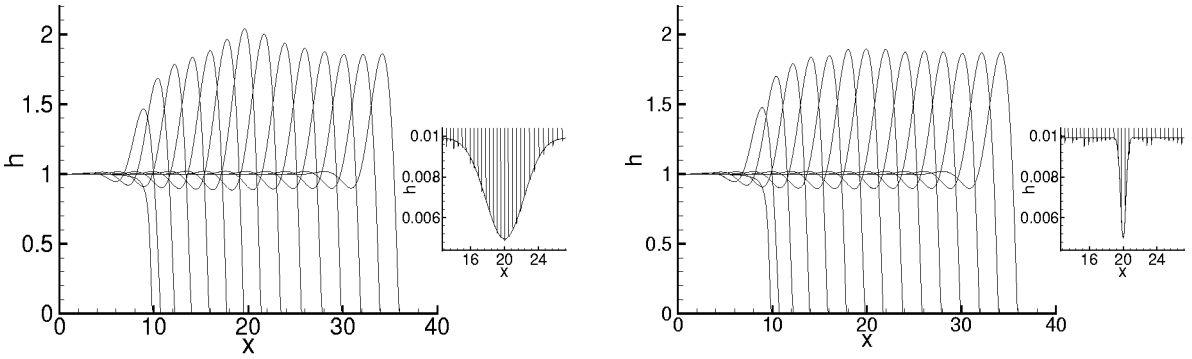

(a) Wide perturbation. (b) Narrow perturbation.

FIG. 4. Snapshot of the 2D fluid profile as it flows over a precursor perturbation. The insets show the zoomed-in perturbation region around $x=20$. The unperturbed precursor thickness is $b=0.01$, barely visible on the scale of the fluid's main body.

the amplification of a perturbation: a precursor's modification on the scale of 1% of the thickness of the fluid's main body leads to a large increase of the capillary ridge's height. However, this occurs only if the perturbation is sufficiently wide. This is illustrated by Fig. 4(b), where the perturbation is of the same depth, but is much more narrow. Here, the fluid practically does not "see" the perturbation. This result is consistent with the solutions describing planarization during spin coating over perturbations (trenches) whose depth is comparable to the thickness of the fluid's main body.[16]

As mentioned in the introduction, 2D simulations deduced the influence of surface perturbations on the instability indirectly, through changing the capillary ridge's height. Therefore, 3D simulations are needed to understand this effect precisely. An issue of particular relevance to applications is the 2D result that a relatively large extent of a perturbation in the streamwise direction is needed to significantly influence the capillary ridge's height and instability; it is not obvious *a priori* that this result can be carried over to 3D geometry.

Therefore, we now proceed to 3D geometry, and analyze the effect that localized perturbations (dips) of the precursor have on the flow stability. For simplicity, we present first the results in large domains, and impose a single perturbation far away from the boundaries, so as to be able to analyze the influence of the perturbation on the flow without being concerned with the boundary conditions. Later, in Sec. V, we consider the interplay between the perturbations of the precursor and the boundary effects.

These perturbations are 3D extensions of the 2D perturbations used in Fig. 4. Figure 5 shows a typical one: There is a flat central region of a given depth, δ (in units of b), and a transition region surrounding the flat part that provides a smooth change from the perturbation's bottom to the unperturbed precursor. These transition regions are needed, since lubrication approximation assumes weak gradients of the fluid thickness, with which a sharp interface between the perturbations and the unperturbed precursor would not be consistent. On the perturbation's sides, the thickness of these transition regions is specified as $b(s)=b[1-\delta\exp(-\Delta_s(s-s_c)^2)]$, where $s=[x, y]$, $\Delta_s=[\Delta_x, \Delta_y]$ defines the width of this transition region, and s_c is the position of a given perturbation's bottom edge. We note that the results are almost insensitive to the particular functional form assigned to $b(s)$, or to the value given to Δ_s. We use $\Delta_s=4$, which gives a reasonable [O(1)] width. In the presentation that follows, we report the total effective perturbation widths, w_x, w_y, as the widths (in the x, y directions) of the regions where the precursor thickness is less than $b(1+\delta)/2$.

Figure 6 shows an example of our results for the flow down a vertical plane ($D=0$), and for unperturbed $b=0.01$. At $t=0$, the time evolution is started from the initial condition obtained from 2D simulations. There are no contact line's perturbations imposed at $t=0$, in contrast to Fig. 2. The precursor perturbation is centered at $x=12$, $y=40$ (therefore, far away from the boundaries), and its effective width is $w_x=w_y=3$. We purposely position the perturbation off center so to avoid imposing any symmetry. In Fig. 6, we see that the fluid's main body flows uniformly under gravity until it reaches the perturbation. There, the flow is slowed down. This slowdown can be understood by recalling that smaller b provides more resistance to the flow in the perturbed regions (note that the $b\to 0$ limit is singular; for $b=0$, the no-slip boundary condition would not permit any contact line's motion). Instead, the fluid escapes to the surrounding, lower resistance regions. In Fig. 6(b), we see that the fluid in these

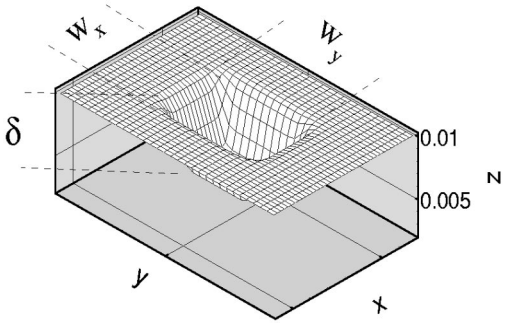

FIG. 5. Zoom-in view of the perturbation characterized by the depth $\delta=0.5$ (in the units of b), and by effective widths $w_x=w_y=3$, as explained in the text.

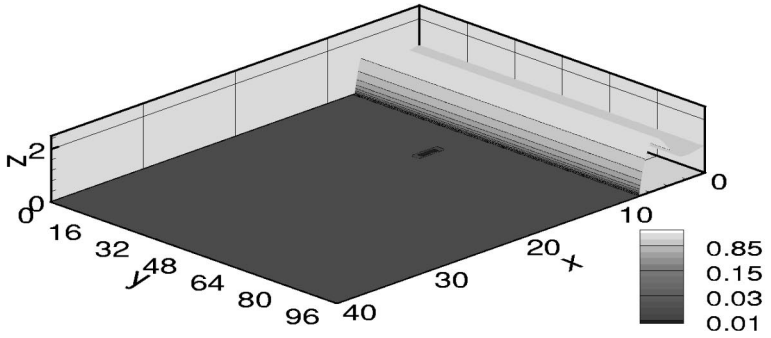

(a) $t = 0$.

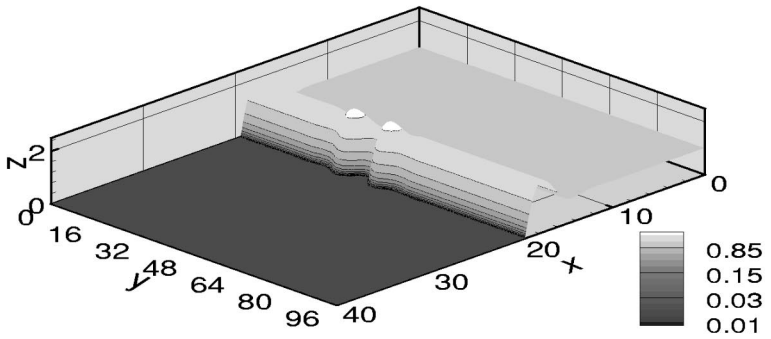

(b) $t = 12$.

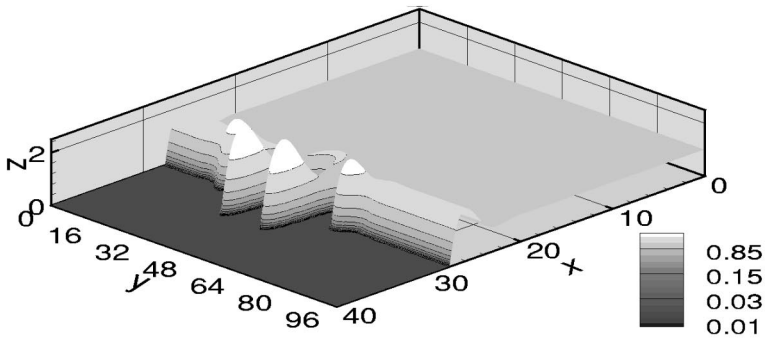

(c) $t = 20$.

FIG. 6. Contour plot of the fluid thickness. The initially flat fluid front shown in (a) flows over perturbed precursor and develops an unstable front shown in the parts (b) and (c). Note how the influence of perturbation propagates in the transverse, y, direction away from the perturbed region. Here $D=0$ and $b=0.01$.

regions (immediately adjacent to the perturbation) is characterized by an increased height of its capillary ridge, while a much smaller capillary ridge is present in the root region, flowing over the perturbation itself. A larger capillary ridge leads to an increase of the fluid velocity (which is approximately proportional to h^2, see, e.g., Ref. 6), and hence to the instability. Figure 6(c) shows the evolving profile at later times, when the instability has already propagated further away from its source.

The fluid profiles shown in Fig. 6, while expected (given the similarity to the profile shown in Fig. 2), are not necessarily obvious from the 2D results, where the capillary ridge is higher as the fluid passes over a perturbation itself (therefore, opposite to the 3D results). There is a major difference between 2D and 3D results: In the 2D case, the fluid does not have the possibility of forming structures in the transverse direction in order to find an energetically more favorable state.

Another interesting question is what determines the speed, u_t, with which information about the presence of perturbation propagates in the transverse direction. In order to answer this question, we analyze first the influence of the size and depth of the perturbation on u_t. One could expect that a stronger "kick" would induce a faster propagation away from the perturbed region. Additional simulations have shown, however, that u_t is independent of the perturbation itself. Therefore, it makes sense to explore the connection of u_t to the general, perturbation independent, features of the flow.

Better insight into this problem can be reached by comparing the propagation of the instability in the flow down a vertical plane ($D=0$) and inclined plane ($D>0$). Figure 7

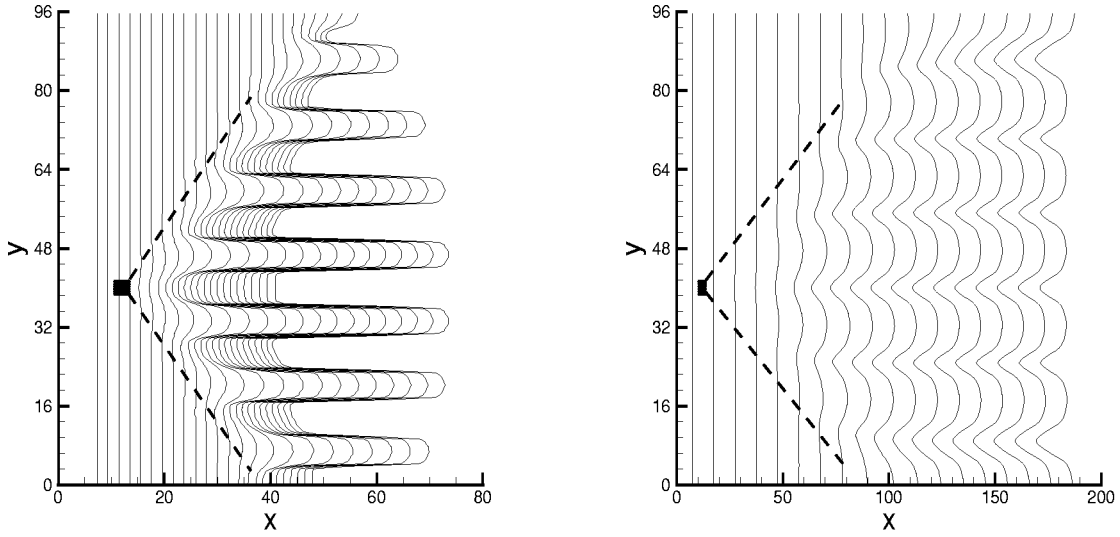

(a) Flow down a vertical plane, $D = 0$; $\delta t = 2$. (b) Flow down an inclined plane, $D = 1$; $\delta t = 10$.

FIG. 7. Snapshots of the fluid profiles in δt intervals. A single perturbation ($w_x = w_y = 3$, $\delta = 0.5$) of the substrate is imposed at $x = 12$, $y = 40$. Note different x-length scales in (a) and (b). The dashed lines are the guides for an eye showing how the instability spreads in the transverse direction.

shows the respective snapshots of fluid profiles, using identical parameters, except for the value of D. These plots allow for a clear comparison of the propagation of the instability in the transverse direction. Using the data plotted in this figure, it is easy to determine u_t for these two cases: $u_t \approx 1.8-2$ for $D=0$, and $u_t \approx 0.5-0.6$ for $D=1$ (illustrated by dashed lines in the figure). Clearly, u_t is a decreasing function of D.

It turns out that u_t can be related to the velocity scale u_l resulting from the LSA of this flow. This velocity is defined by $u_l = \sigma_{max}\lambda_{max}$, i.e., by the product of the maximum value of the growth rate multiplied by the corresponding λ, viz. Fig. 1. The idea is that the instability propagation at the edges of the cones shown in Fig. 7 can be approximately described by the linear picture. Clearly, since this linear approximation ignores rather strong nonlinear effects, one cannot hope for the perfect agreement. Indeed, by performing additional simulations for D's in the range [0, 2], we find that although u_t and u_l are not identical, they are comparable, and, more importantly, they follow the same trend as the value of D is modified. Typically, $u_l/u_t \approx 2.5-3.0$ for all D's explored. The fact that u_l is larger can be explained by recalling that nonlinear effects slow down the growth rate of the instability for later times.[6]

Regarding the flow down an inclined plane, ($D>0$), we note few additional features of the results presented in Fig. 7(b). The emerging patterns' shape is now triangular, as in the case when instability is induced by perturbing the contact line. Also, the distance between the tips is increased, leading to an average wavelength of approximately 16, very similar to the case when the contact line is perturbed directly[5,6] and to the linear stability results mentioned above. This increase of the average distance between patterns can be also seen in the experimental results shown in Fig. 3. We conclude that, at least for the parameters we explore in this work, the main emerging patterns' features—their shape and the distance between tips—are independent of the nature of the perturbation that induces the instability.

IV. EFFECTS OF DISCRETE AND CONTINUOUS PERTURBATIONS

Next, we discuss the instability development in two configurations that are slightly more complicated than a single point perturbation, but are still characterized by large domains and a relatively weak influence of boundary conditions. First, we show how the presence of a number of discrete perturbations influences the instability development; then, we consider continuous perturbations.

A. Discrete perturbations

Figures 8(a) and 8(b) show the fluid profiles' snapshots for the flow, where the precursor thickness is modified by random perturbations. These perturbations are characterized by the widths $w_x = w_y = 3.0 \pm 1.0$, the x positions $x_p = 12.0 \pm 1.0$, the depths $\delta = 0.5 \pm 0.1$, and the distances between perturbations in the y direction 7.0 ± 1.0. We choose a relatively small average distance between perturbations so that the system is not excited by the wavelengths close to λ_{max}. This relatively high-frequency noise forces the system to decide on the emerging wavelengths on its own.

The resulting patterns shown in Fig. 8(a) are very similar to the ones shown in Fig. 2 that resulted from simulations where the contact line itself was perturbed. Additional simulations in which the seed for the random number generator has been modified, confirm that the patterns' shapes, the average wavelengths, and even the wavelengths' variances are very similar in these two kinds of simulations.

In Fig. 8(b), which shows the results for the flow down an inclined plane ($D=1$), the resulting patterns are again very close to those obtained in the simulations where the

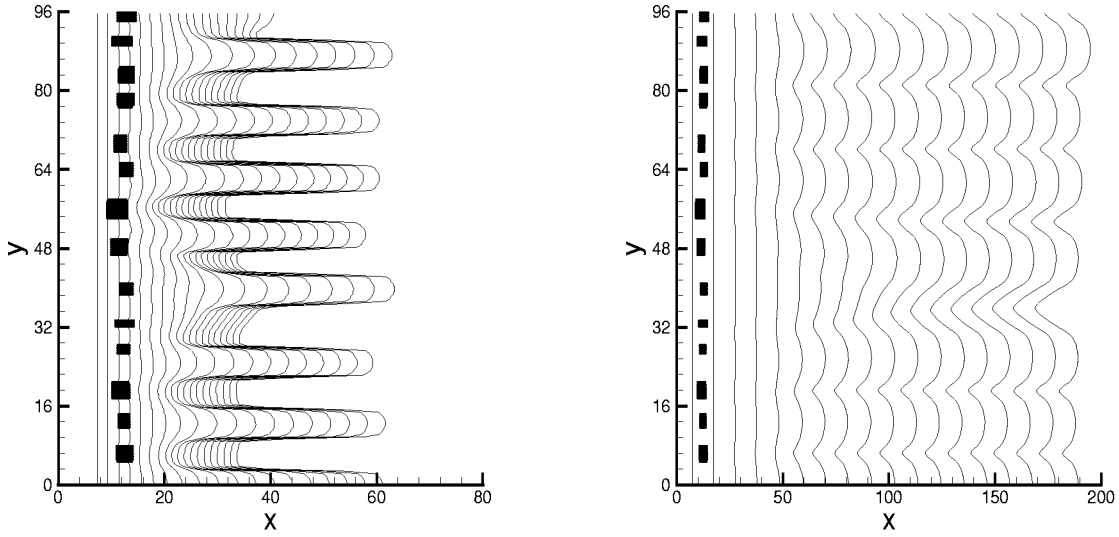

(a) Flow down a vertical plane, $D = 0$; $\delta t = 2$. (b) Flow down an inclined plane, $D = 1$; $\delta t = 10$.

FIG. 8. Snapshots of the fluid profile, where the precursor is perturbed by random perturbations, as explained in the text.

contact line has been perturbed.[5,6] We note that for longer times, the profiles have almost reached a steady state in an appropriate reference frame. This growth saturation has been found for all explored $D>0$, and will discussed in more detail in a separate publication. Similar results have been recently also observed in experiments where thermally driven flows are perturbed by laser pulses, leading to the formation of regular patterns.[46]

B. Continuous perturbations

Until now, we have explored the effect of isolated, point-like perturbations. Here, we briefly discuss instabilities that develop when a nontrivial continuous perturbation that crosses the domain in the transverse direction is present. We will see that the basic picture of the instability development presented so far can be used successfully to understand the formation of rather complex patterns in the configurations that follow.

Figure 9 shows the results for a perturbed region of fixed width ($w_x=3$), where the perturbation is given a sinusoidal shape in the y direction. Although w_x is constant, and it covers the whole domain's width, an instability is still produced, since different film's parts are perturbed at different times. Here, we see three examples of instability caused by these wave-like perturbations. We address first the patterns shown in Fig. 9(b), where the imposed waves period is $p=96/5 \approx 19$. Here, roots develop in the regions where the film reaches the perturbation first, while the tips form in between. Hence, the emerging pattern's wavelength equals the period of imposed perturbation. However, this may not hold in general. For example, in Fig. 9(a), where $p=96$, the roots location is determined by a rather involved interplay between the perturbation and the boundary conditions that requires the formation of a root or a tip at the boundaries (this point is discussed further in Sec. V). Since the fluid is first perturbed (slowed down) close to the boundaries ($y=0,48$), roots form there. Then, two fingers form near the boundaries at a distance determined by the capillary forces. Since the distance between these fingers is large enough to allow for a secondary instability, an additional finger then forms in the domain's center.

Figure 9(c) shows a case where the perturbations' period, $p=96/13 \approx 7.4$, is short enough to cause the formation of patterns that only occasionally follow the rule that the surface perturbation's parts that are reached first and the emerging patterns roots should match. Again, the interplay between the imposed perturbation and boundary conditions leads to a final placement of fingers characterized by an average distance between tips $\lambda=12$.

Figure 10 shows a different kind of perturbation that can lead to instability. Here, a transverse perturbation is kept straight, but its width is modified. This width is varied between 2 and 4, and the period changes from $p=6$ (a) to 12 (b), and 24 (c). First, we note that in the case $p<\lambda_c$, instability cannot develop, since the fluid cannot break the imposed symmetry (similar observation was made in the case of instability imposed by "channels" of low resistance flow in our earlier work[21]). If $p>\lambda_c$, we generally observe formation of tips in regions with narrow perturbation, and of roots where the perturbation is wide [viz. Fig. 10(b)]. If p is as large as in Fig. 10(c), a secondary instability develops (at $y=12$, 36). This is similar to the results shown later (next section) in Fig. 11, where we concentrate more precisely on understanding the influence of boundary conditions.

V. THE INFLUENCE OF BOUNDARY CONDITIONS AND PARAMETRIC DEPENDENCE

There are a number of factors that influence the instability development. First, there are factors related to the basic flow configuration: inclination angle, precursor film thickness, and domain size in the transverse direction. Next, there are parameters introduced by the perturbations: their size,

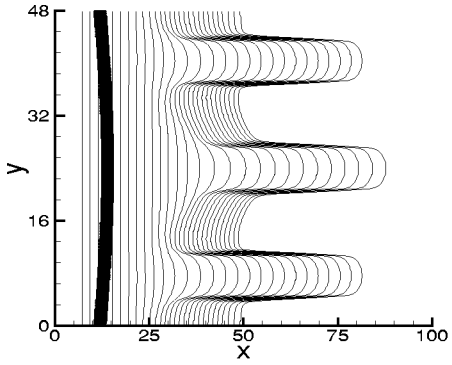

(a) *Period of the perturbation:* $p = 96$.

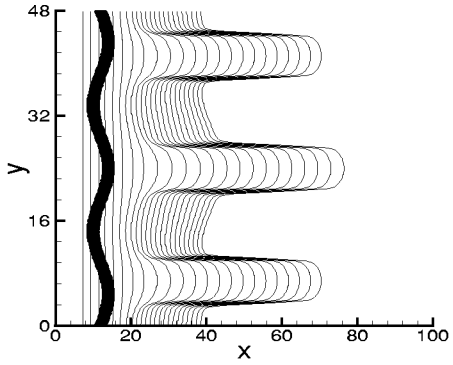

(b) *Period of the perturbation:* $p = 96/5$.

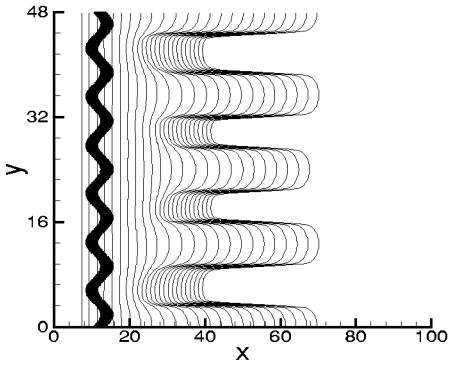

(c) *Period of the perturbation:* $p = 96/13$.

FIG. 9. Snapshots of the fluid profile in $\delta t = 2$ intervals of the flow down a vertical plane where we impose the continuous perturbations, of the width $w_x = 3$, and of various periods in the domain $L_y = 48$.

shape, depth, and distribution. For simplicity and brevity, we discuss here in some detail only two factors: the boundary conditions and the inclination angle. The influence of the other parameters is summarized at the end of this section. If not specified differently, in this section we use $D = 0$, $b = 0.01$, $w_x = w_y = 3$, and $\delta = 0.5$.

A. The interaction between perturbations and boundary conditions

So far, we have mostly avoided discussing the influence of the boundary conditions on the instability development. This influence can indeed be mostly ignored as long as the domain size L_y is large compared to the typical distance between the patterns, i.e., λ_{max} from LSA. However, as soon as $L_y \approx \lambda_{max}$, the boundaries need to be taken into account. We illustrate this point in our computations, but note that the discussion also applies to experiments, where the boundaries are physical walls which typically influence the flow by slowing down the fluid there.

To illustrate the effect of boundaries on pattern formation, we now consider the instability development in a relatively small domain of the width $L_y = 16$, and perturb the flow by a single perturbation. For presentation purposes, we use the fact that our boundary conditions respect "mirror" symmetry and plot results for $0 \leqslant y \leqslant 32$, with the understanding that $y = 16$ is the line of symmetry.

Figure 11 shows how the instability is being modified as the distance between perturbations is decreased from $d = 24$ (a) to 4 (d) (or, equivalently, as the distance from the perturbation to the domain boundary is modified).

First, we realize that the distance between emerging patterns is influenced not only by the spacing d between perturbations, but also by the boundary conditions, which require the formation of either a tip or a root at the boundaries. The interplay between these two factors leads to various λ's, which may or may not be equal to d. However, these emerging λ's do center around λ_{max}. In the examples shown in Fig. 11, the "primary" wavelengths (that develop first) vary between $\lambda = 32/3$ (a) and $\lambda = 16$ (b, c, d). In some cases, additional (secondary) instability develops, such as $\lambda = 8$ in Fig. 11(d). If the distance between the surface perturbations falls below $\lambda_c \approx 8$, there is no pattern formation in between [viz. Fig. 11(d)]. These perturbations do, however, induce instability in the rest of the domain. Since both perturbations are here very close to each other, the mechanism that triggers the instability in this case is somewhat similar to the one ob-

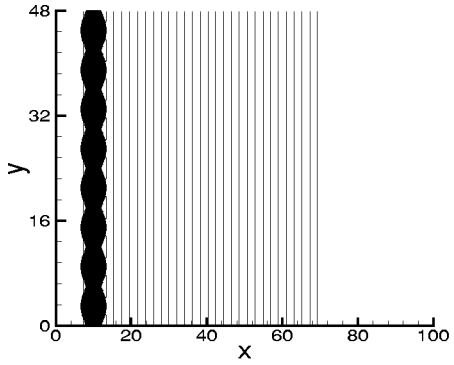

(a) *Period of the perturbation:* $p = 6$.

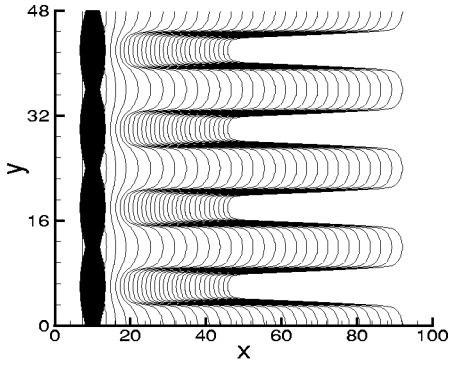

(b) *Period of the perturbation:* $p = 12$.

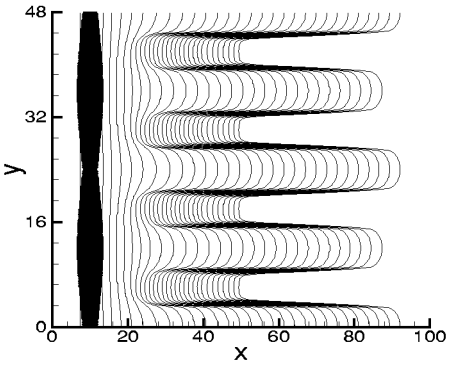

(c) *Period of the perturbation:* $p = 24$.

FIG. 10. Snapshots of the fluid profile in $\delta t = 2$ intervals of the flow down a vertical plane where we impose continuous perturbations of the width $w_x = 2 - 4$, and of various periods in the domain $L_y = 48$.

served with the single perturbation in Sec. IV A. However, now the resulting pattern is modified by the boundary effects.

Still basing our argument on LSA, we can also estimate the growth rates of various patterns. Since, to the leading order, the growth rate is determined by λ, one can predict that the emerging patterns shown in Fig. 11(c) should grow faster than the ones in Fig. 11(a), since the growth rate of $\lambda = 16$ is larger than the one of $\lambda = 32/3$. Also, the patterns shown in Figs. 11(b) and 11(c), grow faster than the ones in Fig. 11(d), since the latter is slowed down by the secondary $\lambda = 8$ instability.

It is also interesting to note the competition between different λ's in Fig. 11(b). Here, $d = 20$ excites the initial formation of two patterns in between the perturbations. These patterns merge into one eventually. However, this merge does not happen in Fig. 11(a), where $d = 24$. Therefore, Figs. 11(a) and 11(b) show that the minimum distance for formation of multiple patterns is between 20 and 24, which is comparable to $2\lambda_c$. These results are consistent with the simulations of the dewetting process on chemically heterogeneous substrates, where the formation of stable patterns is observed when the imposed perturbation is characterized by a lengthscale between λ_c and $2\lambda_c$.[33] Additional simulations (and experiments such as those presented in Sec. VI B) have shown that the exact "critical" distance is influenced by a number of factors, including noise in experiments, and the computational domain's size. See also Ref. 21 for additional discussion regarding this issue.

B. The inclination angle and delayed instability

It is known that changing the inclination angle has a strong influence on the development of the instability.[3,5,6] The patterns' growth is reduced, their shape is changed from finger-like to a triangular sawtooth shape, and the distance between patterns is increased; see Fig. 3 for experimental, and Figs. 7(b) and 8(b) for computational results. Here, we point out one additional feature of the flow down an incline.

Figure 12 shows snapshots of the developed patterns for $D = 0$, 1, 2 and $w_x = w_y = 3$. Obviously, an increase in D has a strong effect; in particular, for $D = 2$, on the considered time scale, the instability is all but completely removed. The weakening of instability as D is increased is as expected from the 2D simulations[34] and experiments.[3] However, careful inspection of Fig. 12(c) shows an interesting additional effect that cannot be deduced from the 2D simulations. For these larger D's, a precursor's perturbation leads to a localized disturbance of the front [barely visible in Fig. 12(c) about time $t = 20$], which "disappears" for an extended period of time, only to start growing again about $t = 150$. This effect

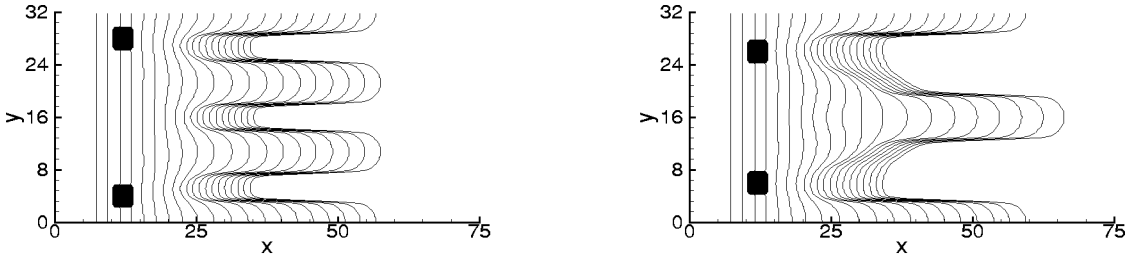

(a) *Distance between perturbations:* $d = 24$. (b) $d = 20$.

(c) $d = 16$. (d) $d = 4$.

FIG. 11. Snapshots of the fluid front as it flows over the perturbations, which are shown by dark areas. The distance between the perturbations, d, is varied as shown in the figures. The fluid front's positions are plotted in $\delta t = 2$ intervals.

can be also seen for $D = 1$ in Figs. 7(b) and 12(b), although the delay is shorter. We hope that this observation of delayed instability will also provide some insight into the still open question of the source of instability for very small inclination angles.

C. The parametric dependence

We have analyzed in some detail the influence of the various perturbation properties on the instability development. For brevity, here we report only the main points:

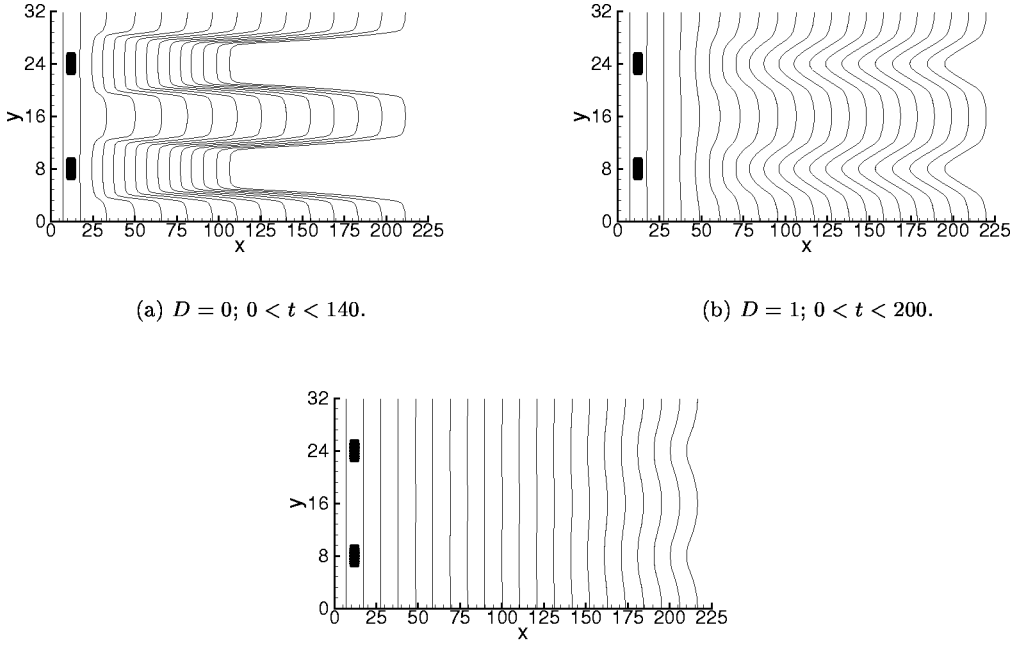

(a) $D = 0$; $0 < t < 140$. (b) $D = 1$; $0 < t < 200$.

(c) $D = 2$; $0 < t < 200$.

FIG. 12. Snapshots of the fluid profile in $\delta t = 10$ intervals for different surface's inclination angles.

(1) *Perturbation width and depth*. Based on the 2D results,[34] we expect a rather strong influence of the perturbation width and depth on the instability. This is really the case: Increasing the perturbed regions' width (both in the x and y directions) and the depth speeds up the development of instability. This effect saturates for large widths and depths, in particular for late times.

(2) *Cumulative effect of multiple perturbations*. Increasing the number of perturbations that follow each other in the streamwise direction has expected influence on the instability development: More perturbations lead to an increased instability. This effect, however, is not very strong, in particular for late times. The limiting case, where all perturbations are touching each other, leading to continuous channels, has already been briefly discussed in a separate publication.[21]

VI. INFLUENCE OF RANDOM SURFACE PERTURBATIONS (NOISE) ON INSTABILITY DEVELOPMENT IN SIMULATIONS AND EXPERIMENTS

In physical experiments, one may expect the presence of random surface noise, due to either mechanical or chemical inhomogeneities. Furthermore, the contact line itself is typically noisy, leading to instabilities, as shown in Fig. 2. So far we have shown that both types of noise lead to the formation of indistinguishable patterns. Therefore, it is sufficient to concentrate on the influence of random surface perturbations on the flow stability and pattern formation. We note that in our simulations these perturbations are characterized by a spatial extend that is much larger than the one that may be expected in the experiments on uniform, carefully prepared surfaces. While it is beyond the scope of this work to analyze computationally any realistic (microscopic) noise, we make a step in this direction by analyzing the influence of randomly distributed perturbations. We show that despite obvious simplifications, these simulations do provide significant insight into the main features of the experimental results.

In this section we concentrate on the following tasks: (1) Analyze an interplay between random and regular perturbations. In particular, show how "better" control may be used to prevent surface perturbations from producing irregular patterns; (2) show experimental results that illustrate the fact that there exists a minimal distance between the imposed perturbations such that the fluid still follows the imposed surface features; and (3) illustrate the effect of noise in experiments.

A. Interaction between noise and regular surface perturbations: Computational results

In an earlier work, we have shown that it is possible to control the instability development by imposing infinite channels of low resistance flow.[21] That result is consistent with the experiments performed using thermally driven flows.[27] In these experiments, a patterned surface (alternating stripes of bare and coated SiO_2) is prepared in a rather elaborate fashion, and the flow is driven by thermocapillary shear stress at the air–liquid interface. Correspondingly, the problem is more complicated (and characterized by much shorter length scales) than the gravity-driven flow outlined here. However, due to the similar nature of the instability in these two problems, one expects that it should be possible to prepare a macroscopic experiment where the stripes are imposed on a (macroscopically) homogeneous surface in some simple manner that allows for relatively straightforward experiments. Examples of such experiments are presented below in Sec. VI B.

We need to point out that in both thermally driven flows, and in the experiments presented here, the fluid *wetting* properties are modified by the externally imposed perturbations. In our simulations, we perturb the *precursor film thickness*, essentially modifying the local resistance to the flow, but implicitly assuming complete wetting. Therefore, the manner in which the perturbations are imposed in our simulations is a simplified version of the physical problem. These precursor film perturbations are also used to simulate additional uncontrolled perturbations (noise) in experiments that could lead to, for example, modifications of the prewetting layer's thickness.

The simplest way to understand the influence of noise is to add a "weak" perturbation to otherwise well-defined flow situation. Following this idea, Fig. 13 shows the results that illustrate some of the effects that noise can have on the flow. The main goal of this figure is to analyze how the "strength" of noise influences the pattern formation. [The terms "strength," as well as "strong" and "weak" below are used in the descriptive sense only. We do not attempt to analyze in detail the relative influence of the parameters characterizing a perturbation (its length, width, depth)]. In Fig. 13 we immediately notice that the flow is very sensitive to the imposed noise's details. This point is made clear already by a simple visual inspection of the different parts of this figure, in which most perturbations appear rather similar. However, the resulting fluid configurations can be very different.

All simulations presented in Fig. 13 are performed in a domain of width $L_y=24$, and have imposed two regular strong perturbations [we refer to them as the perturbations nos. (2) and (3)] characterized by $w_y=3$ (w_x is variable), $\delta=0.5$ and centered at (x,y) coordinates (17, 6), (17, 18), respectively. Without any additional perturbation, (2) and (3) lead to fingers' formation characterized by $\lambda=12$, very similar to the ones shown in Fig. 13(a). In addition to these two perturbations, there is an additional weak perturbation [no. (1)] imposed at $x=10$, $y=12$, that is typically more shallow ($\delta=0.25$), and of decreased width $w_x=w_y$. We think of this perturbation as the "noise" which is of lesser strength than regular perturbations (2) and (3).

Figure 13(a) shows the case where (1) is specified by $w_x=w_y=2.0$, and (2, 3) by $w_x=3.0$. The distance between the perturbations [more precisely, the distance in the streamwise direction between the center of (1) and the starting point of (2, 3)] is $x_d=6$. Here, (1) is not strong enough to modify the flow significantly, so the long time flows development is almost the same as if (1) were not there. In Fig. 13(b), we slightly increase the strength of (1) by choosing $w_x=w_y=2.25$, and keeping everything else the same. This change is sufficient to completely modify the flow: in this case, (1)

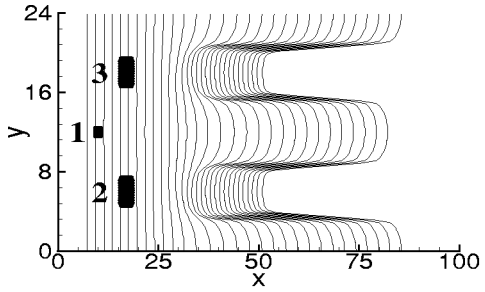

(a) *Weak first perturbation:* (1) $(x = 10)$: $w_x = 2.0$, $\delta = 0.25$; (2, 3) $(x = 17)$: $w_x = 3.0$, $\delta = 0.5$.

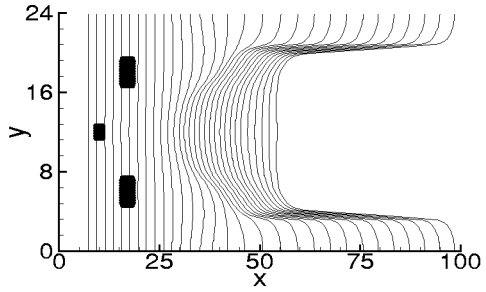

(b) *Strong first perturbation:* (1) $(x = 10)$: $w_x = 2.25$, $\delta = 0.25$; (2, 3) $(x = 17)$: $w_x = 3.0$, $\delta = 0.5$.

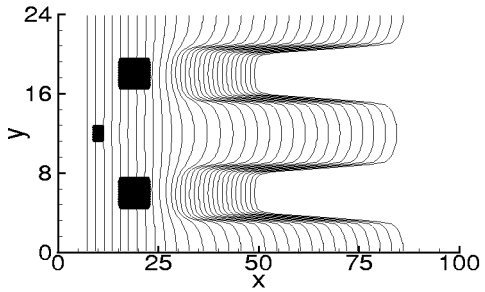

(c) *Long second perturbation:* (1) $(x = 10)$: $w_x = 2.25$, $\delta = 0.25$; (2, 3) $(x = 19)$: $w_x = 7.0$, $\delta = 0.5$.

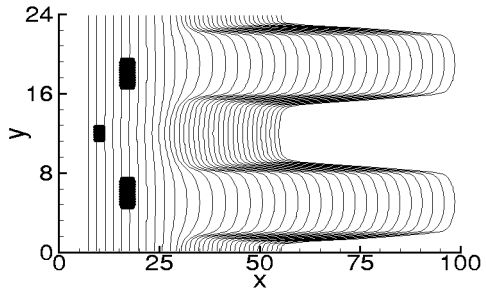

(d) *Deep first perturbation:* (1) $(x = 10)$: $w_x = 2.0$, $\delta = 0.5$; (2, 3) $(x = 17)$: $w_x = 3.0$, $\delta = 0.5$.

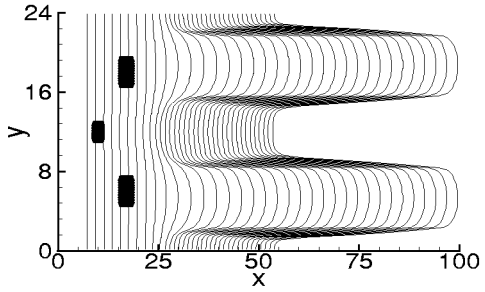

(e) *Large first perturbation:* (1) $(x = 10)$: $w_x = 2.5$, $\delta = 0.25$; (2, 3) $(x = 17)$: $w_x = 3.0$, $\delta = 0.5$.

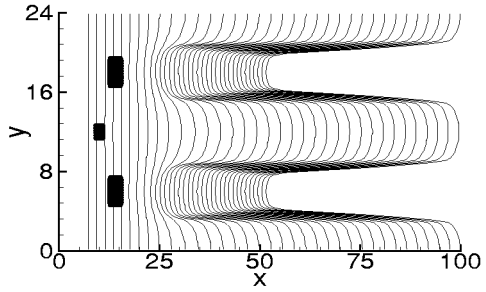

(f) *Short distance between perturbations:* (1) $(x = 10)$: $w_x = 2.25$, $\delta = 0.25$; (2, 3) $(x = 12)$: $w_x = 3.0$, $\delta = 0.5$.

FIG. 13. Snapshots of the fluid profile in $\delta t = 2$ intervals. Here, the flow is perturbed by three perturbations. The first one [referred to as (1)] is always centered at $x = 10$ and its widths in the x and y directions are the same ($w_x = w_y$). The other two perturbations [referred to as (2) and (3)] are identical, have $w_y = 3.0$, $\delta = 0.5$, and are centered at $y = 6$, 18, and at variable x's.

leads to the formation of a root downstream from its position, in contrast to Fig. 13(a). However, the configuration shown in Fig. 13(b) is energetically unfavorable, since the distance between the patterns is much larger than $2\lambda_c$ (see Fig. 11). Therefore, we expect the formation of an additional finger which would reduce λ to 12. The initiation of this splitting process can be seen for the latest times shown in Fig. 13(b).

Figure 13(c) illustrates that "strengthening" of (2, 3) can balance a stronger perturbation (1). Here, (1) is the same as in Fig. 13(b), but the length of (2, 3) is increased to $w_x = 7$, keeping x_d the same. As a result, we reach similar patterns as in the case where (1) was weaker. This is an example of a situation where longer perturbations (similar to the channels analyzed in Ref. 21) lead to the formation of regular patterns that were not achieved by "weaker" pointlike perturbations.

Figure 13(d) returns to the pointlike (2, 3) and explores the influence of the depth of (1). Here, $\delta = 0.5$, while the widths are the same as in Fig. 13(a). This depth's increase has a dramatic influence, and completely modifies the emerging patterns. The result is almost identical as if (2, 3) were absent: two symmetrically positioned fingers develop, the distance between them is $\lambda = 12$, and roots form at the boundaries $(y = 0, 24)$. This configuration is favorable if strong (1)

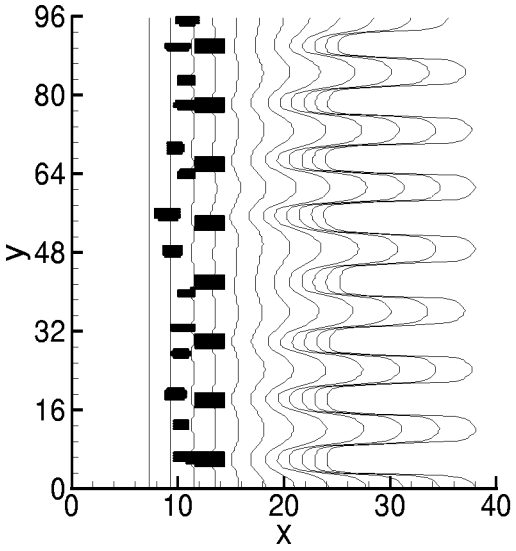

(a) *Short distance between perturbations:* $x_d = 3$.

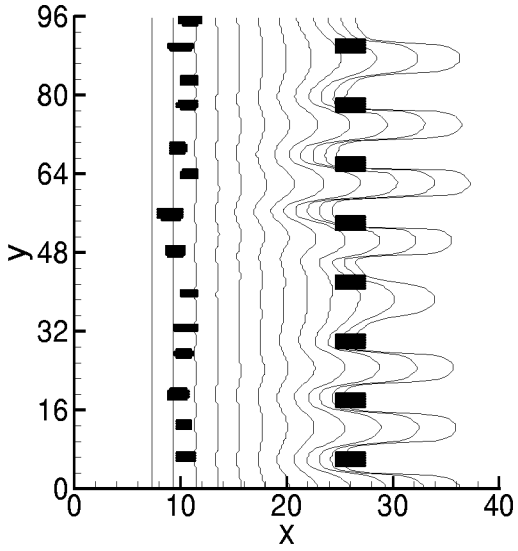

(b) *Long distance between perturbations:* $x_d = 16$.

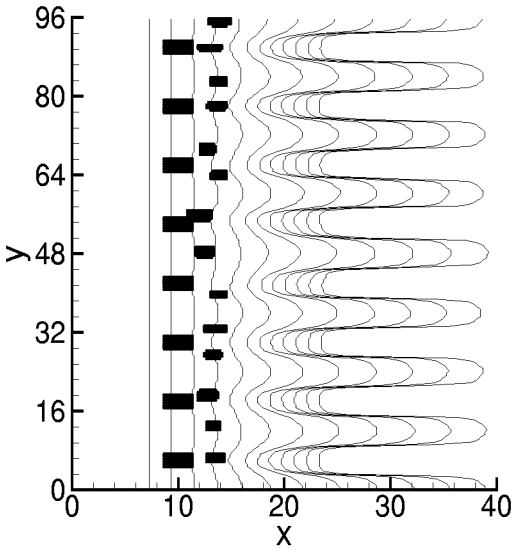

(c) *Random perturbations of perturbed flow:* $x_d = 3$.

FIG. 14. Snapshots of the fluid profile in $\delta t = 2$ intervals. The fluid is perturbed by a combination of regular perturbations [$w_x = w_y = 3.0$, $\delta = 0.5$, at the distance $d = 12$ apart in the y direction, positioned at $x = 26$, 13, 10 in (a), (b), (c), respectively], and random perturbations on average at $x = 10$, 10, 13 respectively. Other details are specified in the text.

prevents the formation of a finger tip in the domain's center at $y = 12$. The same result can be obtained if (1) is kept at the same depth, but its size is increased. This is illustrated in Fig. 13(e), where the size of (1) is increased to $w_x = w_y = 2.5$, but its depth is $\delta = 0.25$. Figures 13(d) and 13(e) therefore illustrate how the spatial extend (w_x, w_y) and the depth, δ, combine to determine the total strength of a perturbation and its influence on the pattern formation process.

Figure 13(f) shows the case where the impact of (1) is weakened by reducing its range of influence. Here, (1, 2, 3) are identical to the ones used in Fig. 13(b), but the centers of (2, 3) are shifted closer to (1), therefore affecting the flow earlier (x_d is decreased from $x_d = 6$ to $x_d = 1$). Since (1) has less time and space to modify the flow, (2,3) take over and lead to the formation of different patterns, compared to the case where the distance between perturbation is larger. A similar effect is also illustrated later in Sec. VI B, regarding the experimental results.

Next, we proceed to more realistic examples of the influence of noise on pattern formation. Figures 14 and 15 combine random perturbations, similar to the ones used in Fig. 8, and perturbations separated in the y direction by a regular distance that is decreased from $d = 12$ in Fig. 14 to $d = 10$ in Fig. 15(a), and to $d = 7$ in Fig. 15(b). The random

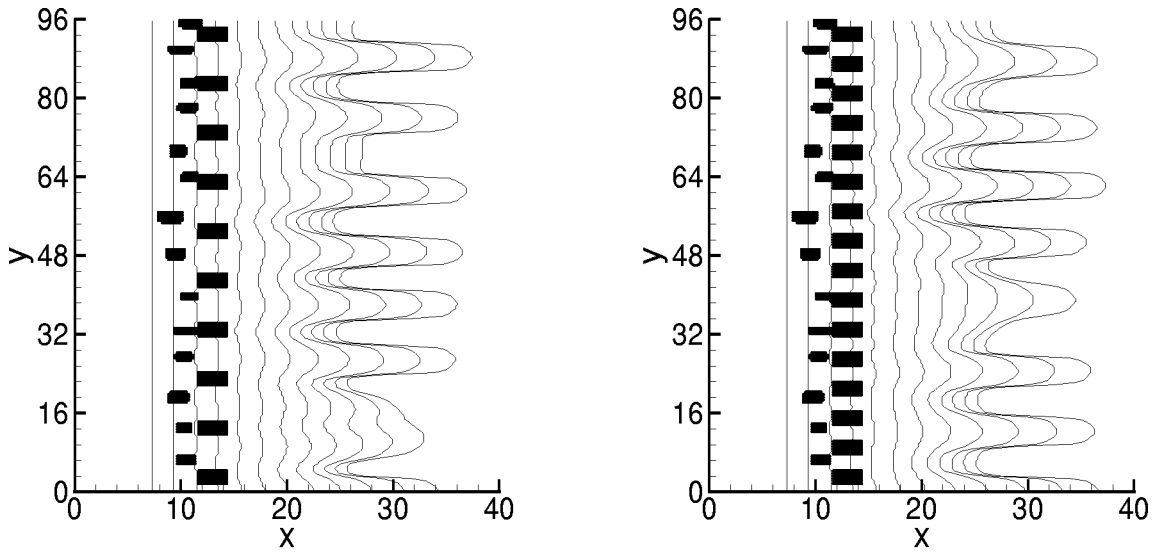

(a) Distance between regular perturbation: $d = 10$. (b) Distance between regular perturbation: $d = 7$.

FIG. 15. Snapshots of the fluid profile in $\delta t = 2$ intervals. The fluid is perturbed by a combination of regular perturbations ($w_x = w_y = 3.0$, $\delta = 0.5$ positioned at $x = 13$), and of random perturbations identical to the ones in Figs. 14(a) and 14(b).

perturbations are weaker than the regular ones and are positioned at an average distance of $d = 7$ ($< \lambda_c$, i.e., in the linearly stable regime). These simulations will be used to directly relate our simulations to experimental results.

In Fig. 14 we use $d = 12$ that is close to the wavelength of maximum growth. Therefore, we expect that these perturbations will strongly influence the flow, leading to regularly spaced patterns characterized by the wavelength that coincides with d. Indeed, this is the case if the random perturbations are placed close to the regular ones, as in Fig. 14(a). Here, the average distance in the streamwise direction between the two rows of perturbations is $x_d = 3$. Therefore, the contact line does not have enough time to develop well-defined patterns prior to reaching the layer of regular perturbations. These regular perturbations then lead to patterns characterized by uniform distance and length. Perhaps surprisingly, these regular patterns are formed rather fast at a relatively short distance downstream from the zone of regular perturbations. If the distance x_d is increased, however, the fluid has more time to develop irregular patterns, and the regular perturbations' influence is not so strong. This effect is shown in Fig. 14(b), where $x_d = 16$. Here, the patterns are less regular compared to Fig. 14(a), although the regular perturbations' influence is still significant. The average wavelength (distance between patterns) is slightly larger than in Fig. 14(a).

Figure 14(c) shows that the fluid that has already been perturbed by regularly spaced surface patterns is much less sensitive to random perturbations, compared to the unperturbed flow. Here, we invert the order of the rows of perturbations and impose regular perturbations first and then a group of random perturbations identical to the ones in Figs. 14(a) and 14(b). The first regular array of perturbations produces uniformly spaced patterns which then reach the random perturbations. These random perturbations are placed close to the regular ones, so that the fluid does not have the time or space to develop long fingers. However, even though the regular patterns are not yet fully formed, they are very stable with respect to this additional disturbance. These results show a quite remarkable stability of the already-formed fluid patterns with respect to surface noise.

Figure 15(a) shows that it is not only the streamwise distance between random and regular perturbations that determines the eventual set of patterns. Here, although the regular perturbations follow the random ones very closely [$x_d = 3$, as in Fig. 14(a)] the influence of these regular perturbations is weakened by the fact that their distance in the y direction is only $d = 10$. Going back to LSA (viz., Fig. 1), we recall that the wavelength $\lambda = 10$ is only weakly unstable. Therefore, these perturbations cannot win against already-formed patterns characterized by, on average, larger (and more unstable) wavelengths. The average distance between patterns is the same as in Fig. 14(b), despite the fact that the regular perturbations are spaced closer to each other.

Figure 15(b) shows the resulting patterns where the distance between regular perturbations is $d = 7$. Since $d = 7$ is less than λ_c, the fluid does not follow the imposed regular perturbations at all, and instead develops randomly distributed patterns. The average distance between the patterns is close to the wavelength of maximum growth, and in this case is the same as in Figs. 14(b) and 15(a).

These computational results allow us to gain better understanding of the influence of noise on the instability development. Next, we use this understanding to explain the results of physical experiments involving flow over patterned surfaces.

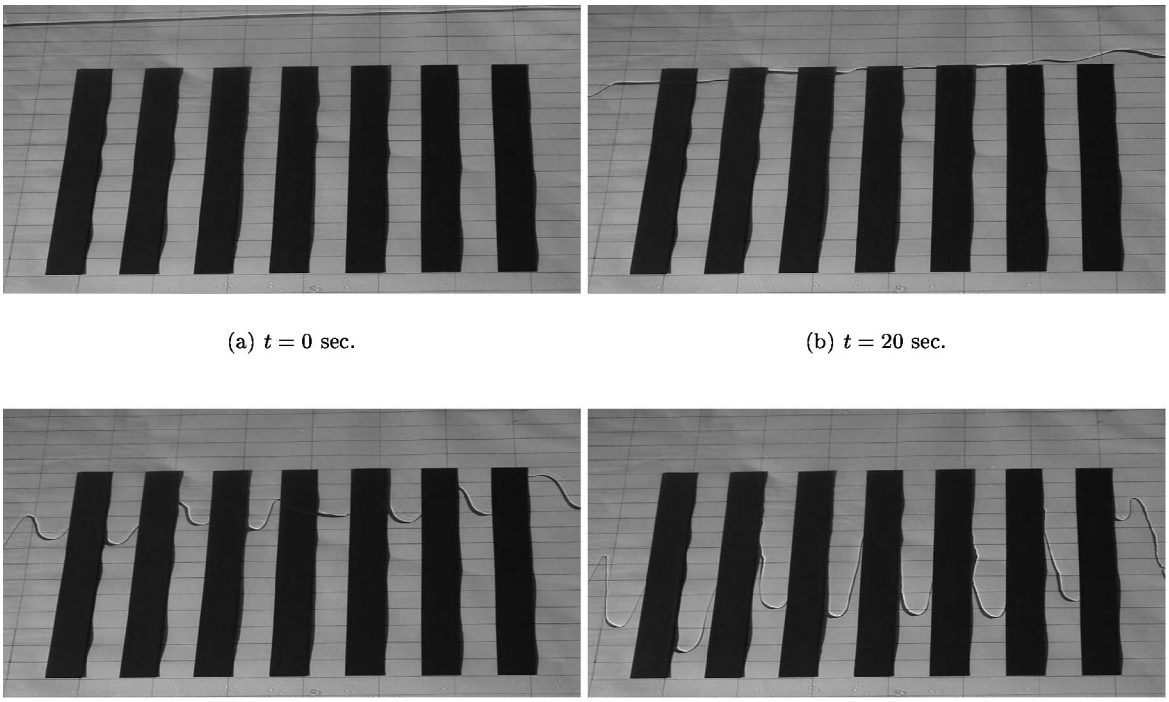

(a) $t = 0$ sec. (b) $t = 20$ sec.

(c) $t = 60$ sec. (d) $t = 180$ sec.

FIG. 16. Snapshots of the PDMS front on 5° incline as it flows over 2.5 cm wide stripes (oil paint), with a spacing of 2.5 cm in between. The fluid is released at time $t=0$, 8 cm above the stripes' start. The amount of fluid is 25 g. Note that the fluid actually flows on the stripes but it is slowed down significantly.

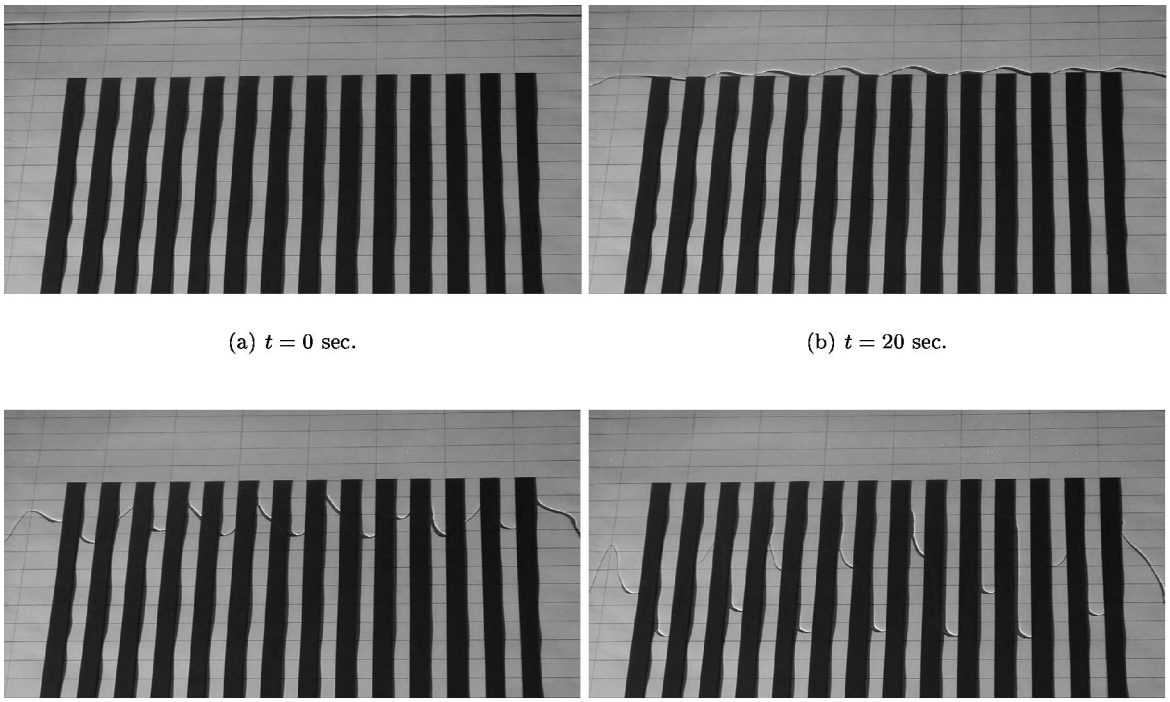

(a) $t = 0$ sec. (b) $t = 20$ sec.

(c) $t = 60$ sec. (d) $t = 180$ sec.

FIG. 17. Snapshots of the PDMS front as it flows over 0.65 cm wide stripes (oil paint), with a spacing of 0.65 cm in between. The setup is the same as in Fig. 16, except for the configuration of stripes.

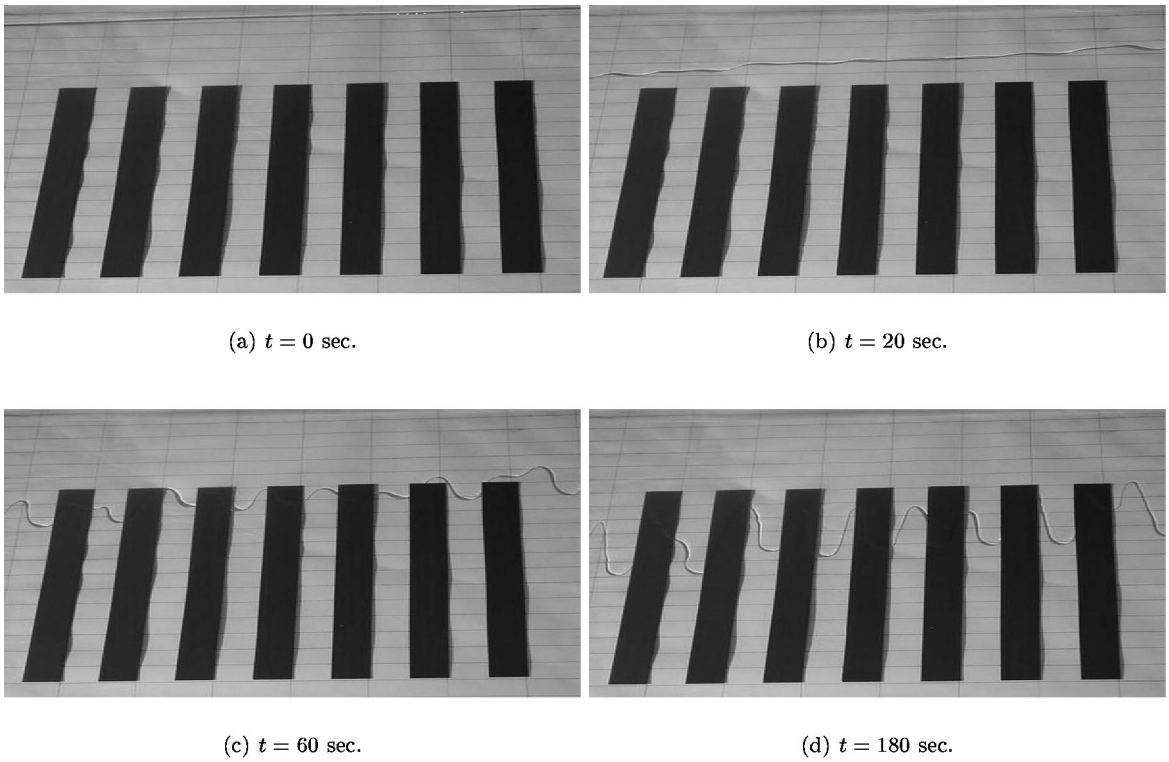

FIG. 18. Snapshots of the PDMS front as it flows over 2.5 cm wide stripes (oil paint), with spacing of 2.5 cm in between. The fluid is released at time $t=0$, 12 cm above the stripes' start. The configuration is identical to the one shown in Fig. 16, except for the release point.

B. Interaction between noise and regular surface perturbations: Experimental results

Figures 16–18 show the experimental patterns that result as PDMS flows over a surface that is modified by the presence of stripes. These stripes are prepared by covering some glass plate's portions with an oil-based paint. Since the apparent contact angle of the PDMS on the stripes is significantly larger than on the glass not covered by the paint, PDMS tries to avoid flowing on the painted stripes and flows in the low-resistance regions instead. The experimental setup is otherwise identical to the one used to obtain the data shown in Fig. 3; therefore, the substrate can be still thought of as covered by a thin prewetted layer. The setup is characterized by small inclination angle $\alpha=5°$, so that the "natural" contact line instability (that would develop on a macroscopically homogeneous surface without any imposed surface perturbations) grows rather slowly and the contact line is only weakly corrugated by the time the fluid reaches the striped region. The imposed stripes modify the flow due to the variation of wetting properties: We have confirmed that wetting properties are relevant by repeating the experiment using identical, but water-based paint stripes—in this case, the fluid flow is unperturbed by the stripes' presence. We note that the fluid actually flows over the stripes (this may not be obvious from the figures due to the insufficient contrast), eventually completely covering the whole domain.

We think of the experiments shown in Figs. 16–18 as an experimental analog of the simulations shown in Figs. 14 and 15. The stripes in experiments play the role of strong, regular perturbations in simulations, while irregular perturbations are naturally provided in experiments by microscopic surface inhomogenities that, for example, may lead to the variations in the thickness of the prewetting film.

Figure 16 shows that the stripes' presence (width of 2.5 cm, and a distance between neighbors of 2.5 cm) is sufficient to induce instability and formation of long fingers in between the stripes [similar to the simulations shown in Fig. 14(a)]. This particular configuration is chosen since the imposed wavelength is close to the natural wavelength that develops in the case of the flow on plane glass, see Fig. 3(c). It is also close to the estimate that goes back to Huppert,[2] who predicts that the emerging wavelength is given by $\lambda_e \approx 7.5[\sqrt{A\sigma}/(\rho g \sin\alpha)]^{1/3}$, where A is the cross-sectional fluid area. With our flow and fluid parameters, this estimate gives $\lambda_e \approx 4.2$ cm. One can show that a similar estimate also results from LSA.

Figure 17 shows that if the distance between stripes is decreased, and everything else is left the same, very different patterns are obtained. Here, the stripes are 0.65 cm wide, and the distance between them is also 0.65 cm. In this case, the fluid follows the imposed perturbations only partially, similar to the computational results shown in Fig. 15(b). Clearly, the average wavelength is much larger than the imposed patterns' periodicity.

Next we proceed to discuss the influence of noise on the flow. This influence was already discussed computationally in Fig. 14, which shows that if the contact line is perturbed by random noise, and then it flows over a striped region, the outcome depends on the distance between the release point and the beginning of this striped region. Figure 18 illustrates

this effect in the experiments. Here, the fluid's release point is 4 cm further upstream from the striped region's beginning, compared to Fig. 16. Clearly, the patterns that form are now much more irregular. Since the instability has more time to develop prior to reaching the striped region, the stripes' influence is not sufficient to reorganize the flow. By performing additional experiments (not shown here for brevity) with different fluid volumes, we have verified that the difference between Figs. 16 and 18 does not result from the change of the fluid thickness at the moment of arriving at the striped region.

Additional experiments have shown that, in some cases, longer stripes could stabilize the flow better than shorter ones, similar to that illustrated in Fig. 13. This applies, in particular, when the imposed distance between the evolving patterns is close to the critical wavelength. We have also analyzed the influence of changing fluid volume. Decreased volume leads to thinner films and shorter length scales, as expected based on simple scaling arguments. This allows, for example, the fluid to follow the stripes as imposed in Fig. 17. This observation is also consistent with the analysis[32] of the dewetting process on heterogeneous substrates.

We conclude this section by noting that we have found very good qualitative agreement between the results of our simulations and experiments. Therefore, the simulations can now be used to predict the main features of the pattern formation, including the effects of noise.

VII. CONCLUSION

Using computational and experimental techniques, we outline the results that allow us to connect natural instability of gravity-driven thin fluid films on macroscopically homogeneous surfaces, and the flow of thin films on patterned surfaces. The natural instability is initiated in simulations by varying, in random fashion, the precursor film thickness, therefore mimicking the surface heterogeneity (noise) in experiments. We find that the patterns that form in the systems where the precursor film is modified are very similar to the ones resulting from contact line perturbations. The flow on patterned surfaces is also modeled by modifying, now in controlled fashion, the precursor film thickness. By imposing local, point-like perturbations, similar results can be produced as in the case of long, channel-like perturbations.

Unperturbed fluid fronts are found to be very sensitive to noise, although significant time can be needed for the front corrugations to start developing, in particular for small inclination angles. However, if fluid has already-formed patterns, they are almost insensitive to the random perturbations of the surface. This conclusion has been reached both in simulations and in experiments.

Our theoretical and computational methods are currently being developed to include the modeling of the details of (possibly heterogeneous) surface chemistry. However, the present model already shows a lot of potential, since it has successfully reproduced the qualitative features of experimentally observed pattern formation in the experiments reported here, as well as of the experiments involving thermally driven thin films. Our future work will proceed in the direction of developing a better understanding of the relevant issues that determine the dynamics of microflows, including their control and applications.

ACKNOWLEDGMENTS

L.K. acknowledges help with experiments by an undergraduate student of NJIT, Rafal Turek, and thanks Gregory Kriegsman for help with student summer support. The authors acknowledge support by NSF Grant No. INT-0122911. J.D. acknowledges support from Consejo Nacional de Investigaciones Científicas y Técnicas (CONICET-Argentina).

[1] N. Silvi and E. B. Dussan, "On the rewetting of an inclined solid surface by a liquid," Phys. Fluids **28**, 5 (1985).
[2] H. Huppert, "Flow and instability of a viscous current down a slope," Nature (London) **300**, 427 (1982).
[3] M. F. G. Johnson," Experimental study of rivulet formation on an inclined plate by fluorescent imaging," Ph.D. thesis, Northwestern University, 1997.
[4] M. F. G. Johnson, R. A. Schluter, M. J. Miksis, and S. G. Bankoff, "Experimental study of rivulet formation on an inclined plane by fluorescent imaging," J. Fluid Mech. **394**, 339 (1999).
[5] J. Diez and L. Kondic, "Contact line instabilites of thin liquid films," Phys. Rev. Lett. **86**, 632 (2001).
[6] L. Kondic and J. Diez, "Contact line instabilities of thin film flows: Constant flux configuration," Phys. Fluids **13**, 3168 (2001).
[7] S. M. Troian, E. Herbolzheimer, S. A. Safran, and J. F. Joanny, "Fingering instabilities of driven spreading films," Europhys. Lett. **10**, 25 (1989).
[8] M. A. Spaid and G. M. Homsy, "Stability of Newtonian and viscoelastic dynamic contact lines," Phys. Fluids **8**, 460 (1996).
[9] A. L. Bertozzi and M. P. Brenner, "Linear stability and transient growth in driven contact lines," Phys. Fluids **9**, 530 (1997).
[10] Y. Ye and H. Chang, "A spectral theory for fingering on a prewetted plane," Phys. Fluids **11**, 2494 (1999).
[11] R. O. Grigoriev, "Contact line instability and pattern selection in thermally driven liquid films," Phys. Fluids **15**, 1363 (2003).
[12] J. M. Davis and S. M. Troian, "On a generalized approach to the linear stability of spatially nonuniform thin film flows," Phys. Fluids **15**, 1344 (2003).
[13] S. Kalliadasis, C. Bielarz, and G. M. Homsy, "Steady free-surface thin film flows over topography," Phys. Fluids **12**, 1889 (2000).
[14] C. Bielarz and S. Kalliadasis, "Time-dependent free-surface thin film flows over topography," Phys. Fluids **15**, 2512 (2003).
[15] J-C. Baret and M. M. J. Decré, "Gravity-driven flows of viscous liquids over two-dimensional topographies," J. Fluid Mech. **487**, 147 (2003).
[16] L. E. Stillwagon and R. G. Larson, "Leveling of thin films over uneven substrates during spin coating," Phys. Fluids A **2**, 1937 (1990).
[17] K. Hoffmann, B. Wagner, and A. Münch, "On the generation and spreading of 'finger' instabilities in film coating processes," in *Lecture Notes in Computational Science and Engineering*, Vol. 3, edited by H. J. Bungartz, F. Dust, and C. Zenger (Springer, Berlin, 1999).
[18] C. Y. Wang, "Flow over surfaces with parallel grooves," Phys. Fluids **15**, 1114 (2003).
[19] L. M. Hocking, "A moving fluid interface on a rough surface," J. Fluid Mech. **76**, 801 (1976).
[20] M. J. Miksis and S. H. Davis, "Slip flow over rough and coated surfaces," J. Fluid Mech. **273**, 125 (1994).
[21] L. Kondic and J. Diez, "Flow of thin films on patterned surfaces: Controlling the instability," Phys. Rev. E **65**, 045301 (2002).
[22] J. Drelich, J. L. Wilbur, J. D. Miller, and G. M. Whitesides, "Contact angles for liquid drops at a model heterogenous surface consisting of alternating and parallel hydrophobic/hydrophylic strips," Langmuir **12**, 1913 (1996).
[23] L. W. Schwartz, "Hysteretic effects in droplet motions on heterogenous substrates: Direct numerical simulations," Langmuir **14**, 3440 (1998).
[24] L. W. Schwartz and R. R. Eley, "Simulation of droplet motion of low-energy and heterogenous surfaces," J. Colloid Interface Sci. **202**, 173 (1998).
[25] S. Brandon, N. Haimovich, E. Yeger, and A. Marmur, "Partial wetting of chemically patterned surfaces: The effect of drop size," J. Colloid Interface Sci. **263**, 237 (2003).

[26]U. Öpik, "Contact-angle hysteresis caused by a random distribution of weak heterogeneities on a solid surface," J. Colloid Interface Sci. **223**, 143 (2000).
[27]D. E. Kataoka and S. M. Troian, "Patterning liquid flow on the microscopic scale," Nature (London) **402**, 794 (1999).
[28]A. A. Darhuber, S. M. Troian, S. M. Miller, and S. Wagner, "Morphology of liquid microstructures on chemically patterned surfaces," J. Appl. Phys. **87**, 7768 (2000).
[29]A. A. Darhuber, S. M. Troian, J. M. Davis, S. M. Miller, and S. Wagner, "Selective dip-coating of chemically micropatterned surfaces," J. Appl. Phys. **88**, 5119 (2000).
[30]A. A. Darhuber, S. M. Troian, and W. W. Reisner, "Dynamics of capillary spreading along hydrophylic microstripes," Phys. Rev. E **64**, 031603 (2001).
[31]N. Garnier, R. O. Grigoriev, and M. F. Schatz, "Optical manipulation of microscale fluid flow," Phys. Rev. Lett. **91**, 054501 (2003).
[32]L. Brusch, H. Kühne, U. Thiele, and M. Bär, "Dewetting of thin films on heterogenous substrates: Pinning versus coarsening," Phys. Rev. E **66**, 011602 (2002).
[33]K. Kargupta and A. Sharma, "Templating of thin films induced by dewetting on patterned surfaces," Phys. Rev. Lett. **86**, 4536 (2001).
[34]L. Kondic and A. L. Bertozzi, "Nonlinear dynamics and transient growth of driven contact lines," Phys. Fluids **11**, 3560 (1999).
[35]A. L. Bertozzi, G. Grün, and T. P. Witelski, "Dewetting films: bifurcations and concentrations," Nonlinearity **14**, 1569 (2001).
[36]K. B. Glasner and T. P. Witelski, "Coarsening dynamics of dewetting films," Phys. Rev. E **67**, 016302 (2003).
[37]L. M. Pismen and Y. Pomeau, "Disjoining potential and spreading of thin liquid layers in the diffuse-interface model coupled to hydrodynamics," Phys. Rev. E **62**, 2480 (2000).
[38]U. Thiele, M. G. Velarde, K. Neuffer, and Y. Pomeau, "Film rupture in the diffuse interface model coupled to hydrodynamics," Phys. Rev. E **64**, 031602 (2001).
[39]J. Diez and L. Kondic, "Computing three-dimensinal thin film flows including contact lines," J. Comput. Phys. **183**, 274 (2002).
[40]H. P. Greenspan, "On the motion of a small viscous droplet that wets a surface," J. Fluid Mech. **84**, 125 (1978).
[41]E. B. Dussan, "The moving contact line: The slip boundary condition," J. Fluid Mech. **77**, 665 (1976).
[42]L. M. Hocking and A. D. Rivers, "The spreading of a drop by capillary action," J. Fluid Mech. **121**, 425 (1982).
[43]J. Diez, L. Kondic, and A. L. Bertozzi, "Global models for moving contact lines," Phys. Rev. E **63**, 011208 (2001).
[44]L. Kondic, "Instabilities in the flow of thin liquid films," SIAM Rev. **45**, 95 (2003).
[45]P. G. de Gennes, "Wetting: Statics and dynamics," Rev. Mod. Phys. **57**, 827 (1985).
[46]T. Witelski and J. Sur (private communication, 2003).